

HYBRID CONTROL FOR MOTION SYSTEMS WITH IMPROVED DISTURBANCE REJECTION

Marcel Heertjes

ASML
Mechatronic Systems Development
5600 MD Veldhoven, The Netherlands
marcel.heertjes@asml.com

Xander Schuurbiers

Eindhoven University of Technology
Faculty of Mechanical Engineering
5600 MD Eindhoven, The Netherlands
x.g.p.schuurbiers@student.tue.nl

Henk Nijmeijer

Eindhoven University of Technology
Faculty of Mechanical Engineering
5600 MD Eindhoven, The Netherlands
h.nijmeijer@tue.nl

Abstract

In this paper a hybrid control design for motion systems is proposed that aims at improved disturbance rejection under equal noise response. Typically performance-relevant frequency contributions in the error response are up-scaled through linear filtering, subjected to a nonlinear weighting, that is, inducing extra controller gain when large enough and otherwise neglected, and subsequently down-scaled as to maintain closed-loop stability. At a wafer stage of an industrial wafer scanner such a strategy is demonstrated to improve low-frequent disturbance suppression while limiting the amplification of high-frequent noise.

Key words

Absolute Stability, Inherent Design Limitations, Lyapunov Stability, Nonlinear Control, Wafer Scanners.

1 Introduction

Over the past decades the semiconductor industry faced a constant miniaturization but growing complexity of its integrated circuits (ICs). The chip dimensions shrink while their functional abilities expand. To cope with such miniaturization, positioning systems incorporated in industrial wafer scanners highly evolved in terms of (electro-)mechanics, optics, and sensors. The usage of intelligent control strategies such as learning (Heertjes and Tso, 2007; Misha, Coaplen, and Tomizuka, 2007), nonlinear (Heertjes and Van de Wouw, 2006), adaptive, or multi-variable control (Van de Wal, *et al.*, 2002) cannot fall behind.

In terms of intelligent control, a hybrid control design is proposed for motion systems in general but high-speed (wafer) stages in particular. The design aims at improved disturbance rejection under equal noise response. Key is the introduction of a nonlinear controller gain used to adapt the inherent trade-off between disturbance rejection and measurement noise sensitivity (Freudenberg, *et al.*, 2003). If the response

contains frequency contributions sufficiently below the controller bandwidth then servo performance benefits from increased controller gain. Contrarily, beyond the bandwidth an increased gain often induces the amplification of high-frequent noise.

By monitoring the signals at hand and act accordingly, the choice for a nonlinear controller such as used in (Heertjes, *et al.*, 2005) can significantly improve upon servo performance. In a similar control setting, a performance-based nonlinear filtering strategy is proposed in which we distinguish three steps. In the first step, performance-relevant frequency content, if present in the servo error signals, is up-scaled using a linear bandpass filter operation. In the second step, an amplitude-based deadzone operation is performed, which can be seen as a (weighted) selection between applying extra feedback or not. In the third step, the bandpass filter operation is inverted as to preserve stability of the underlying nonlinear closed-loop system.

The resulting hybrid control design combines three functions: monitoring by lifting the frequency content of interest temporarily from the error signals at hand, selection by (nonlinear) weighting of the lifted error signals, and loop shaping to keep the closed-loop stability result valid. Different from this loop shaping, the monitoring function, for example, is long used in the field of audio applications, see, for example, (Schafer, Oppenheim, and Stockham, 1968). Also, the selection function is known (Aangenent, Van de Molengraft, and Steinbuch, 2005; Beak, Chung, and Tomizuka, 2006; Armstrong, *et al.*, 2006). The combination, however, is unknown to the authors.

This paper is organized as follows. In Section 2, the hybrid control design is presented in the context of motion systems. This includes an absolute stability argument. In Section 3, the dynamics and control of wafer scanners is discussed, which serves as an experimental benchmark. In Section 4 performance is assessed on a wafer stage of a wafer scanner. In Section 5, a brief summary of the main conclusions is given.

2 Hybrid Control Design

In presenting a hybrid control design for motion systems, we distinguish between a nominal linear control design and an extra nonlinear controller. The nominal design aims at both robust stability and performance. The extra nonlinear controller is used to improve upon the low-frequency disturbance rejection properties without transmitting too much high-frequency noise. That is, on the occurrence of performance-limiting oscillations, the linear controller is given extra controller gain. Because of the incidental nature in which these oscillations are assumed to occur, the amplification of noise (mostly under low-gain feedback) is kept limited. In this context, we refer to hybrid control as the (continuous) switching between the dynamics corresponding to the nominal control design and the dynamics induced by the extra nonlinear controller.

A schematics of a nominal controlled motion system is depicted in the block diagram of Figure 1. Given

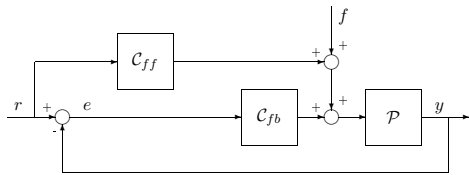


Figure 1. Schematics of a nominal controlled motion system.

a reference command r , a servo error signal e is constructed using the relation $e = r - y$ where y represents the output of the plant \mathcal{P} . The error signal e is fed into a feedback controller C_{fb} that aims at disturbance rejection in view of set-point disturbances r and force disturbances f . To obtain sufficient tracking accuracy, a feedforward controller C_{ff} is added.

Toward improved low-frequency tracking without the usual amplification of high-frequency noise, the linear feedback connection in Figure 1 is given an extra nonlinear path, see Figure 2, in which we distinguish three

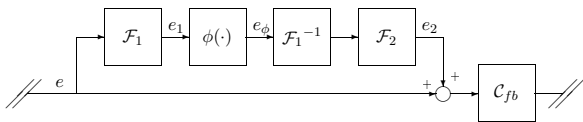


Figure 2. Schematics of the overall nonlinear controller.

functions: monitoring, selection, and loop-shaping.

A monitoring function is given to the filter structure \mathcal{F}_1 which aims at lifting the (low-)frequency content of possibly performance limiting oscillations contained in e . A logical choice for such a filter structure would

typically be a single notch filter operation of the form

$$\mathcal{F}_1(s) = \frac{s^2 + 2\beta_z\omega_z s + \omega_z^2}{s^2 + 2\beta_p\omega_p s + \omega_p^2}, \quad (1)$$

where $\beta_z > \beta_p$ representing the dimensionless damping coefficients and $\omega_z = \omega_p$ the zero and pole frequencies. Hence narrow-band amplification.

A selection function is given to the (nonlinear) weighting of the lifted error signals by $\phi(\cdot)$. The memoryless operation $\phi(\cdot)$ is given by a deadzone nonlinearity of the form

$$\phi(e_1) = \begin{cases} 0, & \text{if } |e_1| \leq \delta, \\ 1 - \frac{\delta}{|e_1|}, & \text{if } |e_1| > \delta, \end{cases} \quad (2)$$

with δ a deadzone length. $\phi(\cdot)$ is sector-bounded in the sense that $0 \leq \phi(\cdot) \leq 1$. If performance-limiting oscillations are sufficiently present in the lifted error response e_1 , then extra controller gain is induced. Contrarily, if e_1 does not contain such oscillations, then no extra gain is induced thus avoiding the extra amplification of noise by feedback.

A loop shaping function is given to the filter structure \mathcal{F}_2 , see (Heertjes, *et al.*, 2005), from which we adopt

$$\begin{aligned} \mathcal{F}_2(s) &= \alpha \cdot \frac{s^2 + 2\beta_z\omega_z s + \omega_z^2}{s^2 + 2\beta_p\omega_p s + \omega_p^2} \cdot \frac{\omega_{lp}^2}{s^2 + 2\beta_{lp}\omega_{lp} s + \omega_{lp}^2}, \end{aligned} \quad (3)$$

with α a stability-limited extra gain ratio, $\omega_z = \omega_p$ the zero and pole breakpoints of a notch filter, $\beta_z < \beta_p$ the corresponding dimensionless damping coefficients, ω_{lp} the breakpoint of a second-order low-pass filter and β_{lp} its dimensionless damping coefficient.

Closed-loop stability of the hybrid controlled dynamics is sufficiently guaranteed using the following result.

Theorem 2.1. *Assume the strictly proper system \mathcal{P} in Figure 1 that is stabilized – under bounded disturbances r and f – by C_{fb} which is strictly proper and Hurwitz. Also assume \mathcal{F}_1 and \mathcal{F}_2 in Figure 2 to be stable and proper. Then any controller of the form $(1 + \mathcal{F}_1\phi(\cdot)\mathcal{F}_1^{-1}\mathcal{F}_2)C_{fb}$ with $0 \leq \phi(\cdot) \leq 1$ stabilizes \mathcal{P} if*

$$\begin{aligned} \Re \{ \mathcal{F}_1^{-1}(j\omega)\mathcal{F}_2(j\omega) S_c(j\omega)\mathcal{F}_1(j\omega) \} = \\ \Re \{ \mathcal{F}_2(j\omega) S_c(j\omega) \} \geq -1, \end{aligned} \quad (4)$$

with

$$S_c(j\omega) = \frac{C_{fb}(j\omega)\mathcal{P}(j\omega)}{1 + C_{fb}(j\omega)\mathcal{P}(j\omega)}. \quad (5)$$

For a proof we refer to the results in (Heertjes, *et al.*, 2005) which are derived from absolute stability theory (Yakubovich, Leonov, and Gelig, 2004). Since the application of \mathcal{F}_1 with its exact inverse \mathcal{F}_1^{-1} is invariant under the result in (4), it provides us with the means to discriminate between performance-limiting oscillations and not on the basis of the frequency content of these oscillations. As such, a strictly performance-based filter operation is obtained to effectively deal with such oscillations. This will be demonstrated on a wafer stage of a wafer scanner.

3 Dynamics and Control of Wafer Scanners

A schematic representation of a wafer scanner is shown in Figure 3. Light from a laser passes a reti-

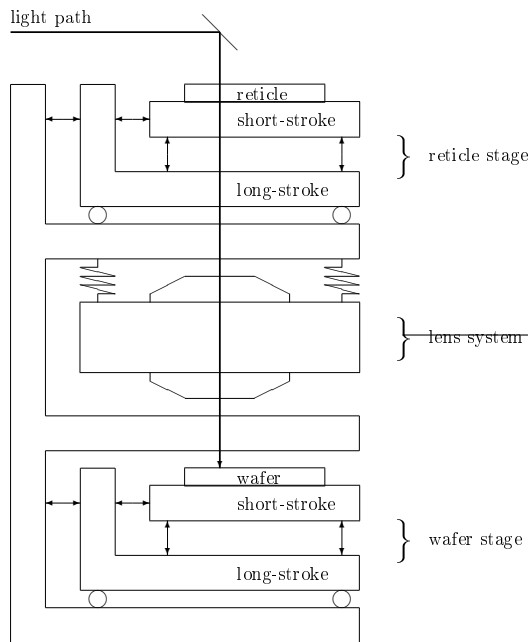


Figure 3. Schematic of a wafer scanner.

cle – a quartz plate containing the image – through a lens, which reduces the desired image by a factor of four, and onto a wafer. The latter is represented by a silicon disk of 300 mm in diameter. Both reticle and wafer are part of two separate motion controlled sub-systems: the reticle stage and the wafer stage each employing a dual-stroke strategy. A long-stroke is used for fast large-range motions whereas a short-stroke is used for accurate but small-range tracking. The short-stroke stages are represented by floating masses which are controlled in six degrees-of-freedom.

For the z -direction of the short-stroke wafer stage, the single-input single-output linear feedback design can be represented by the simplified block diagram representation of Figure 1. In transfer function notation, the wafer stage plant is given by the following simplified

fourth-order model

$$\mathcal{P}(s) = \frac{m_1 s^2 + b_{12} s + k_{12}}{m_1 m_2 s^4 + b_{12} (m_1 + m_2) s^3 + k_{12} (m_1 + m_2) s^2}, \quad (6)$$

with $m_1 + m_2 \approx 22.5$ kg representing the wafer stage mass. High-frequency resonance is modelled via the distinction between $m_1 \approx 5$ kg and $m_2 \approx 17$ kg, an interconnected stiffness coefficient $k_{12} = 7.5 \cdot 10^7$ Nm⁻¹, and corresponding damping coefficient $b_{12} = 9 \cdot 10^1$ Nsm⁻¹.

The validity of the model (with sampling delay correction) is shown in Figure 4. It shows frequency response functions of both (electro-)mechanics and model. Below 20 Hz, a poor measurement qual-

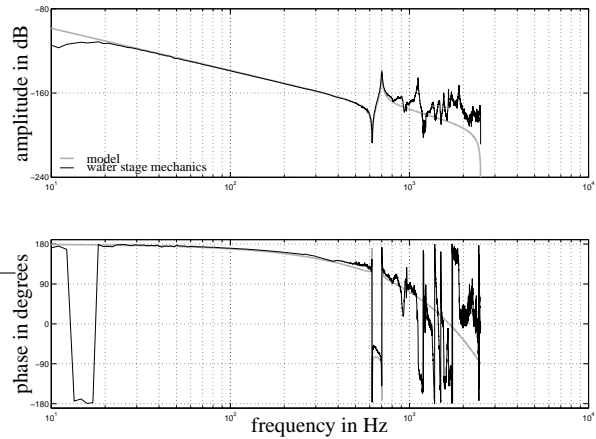


Figure 4. Bode diagram of the measured (electro-)mechanics in z -direction along with the characteristics of a fourth-order model.

ity induces a poor correspondence between measurement and simulation; all measurements are done under closed-loop conditions. Beyond 1 kHz, higher-order dynamics no longer justify the model assumptions.

The feedback controller \mathcal{C}_{fb} in Figure 1 is based on a series connection of a proportional-integrator-derivative (PID) controller which aims at disturbance rejection and robust stability, a second-order low-pass filter to avoid high-frequent noise amplification, and three notch filters designed to counteract higher-order plant resonances. In transfer function notation, the simplified model reads

$$\mathcal{C}_{fb}(s) = \mathcal{F}_{pid}(s) \mathcal{F}_{lp}(s) \mathcal{F}_{n,1}(s) \mathcal{F}_{n,2}(s) \mathcal{F}_{n,3}(s), \quad (7)$$

with

$$\mathcal{F}_{pid}(s) = \frac{k_p (s^2 + \omega_d s + \omega_i \omega_d)}{\omega_d s}, \quad (8)$$

$k_p = 6.9 \cdot 10^6 \text{ Nm}^{-1}$ a loop gain, $\omega_d \approx 3.8 \cdot 10^2 \text{ rad s}^{-1}$ the cut-off frequency of a differential operation, and $\omega_i \approx 3.14 \cdot 10^2 \text{ rad s}^{-1}$ the cut-off frequency of an integral operation,

$$\mathcal{F}_{lp}(s) = \frac{\omega_{lp}^2}{s^2 + 2\beta\omega_{lp}s + \omega_{lp}^2}, \quad (9)$$

$\omega_{lp} \approx 3.04 \cdot 10^3 \text{ rad s}^{-1}$ the cut-off frequency of a second-order low-pass filter, $\beta \approx 0.08$ a dimensionless damping coefficient, and three notch filters having a general second-order filter structure, or

$$\mathcal{F}_{n,i}(s) = \left(\frac{\omega_{p,i}}{\omega_{z,i}} \right)^2 \cdot \frac{s^2 + 2\beta_{z,i}\omega_{z,i}s + \omega_{z,i}^2}{s^2 + 2\beta_{p,i}\omega_{p,i}s + \omega_{p,i}^2}. \quad (10)$$

The parameter values used for the notch filters are given in Table 1.

i	$\omega_{z,i}$ in rad s^{-1}	$\beta_{z,i}$	$\omega_{p,i}$ in rad s^{-1}	$\beta_{p,i}$
1	90π	0.4	96π	0.05
2	1456π	$1.53 \cdot 10^{-6}$	1624π	0.88
3	2207π	0.19	1459π	0.18

Table 1. Notch filter parameter values.

Both plant \mathcal{P} and controller \mathcal{C}_{fb} are characterized by the open-loop frequency response functions such as depicted in Figure 5. In Bode representation it shows

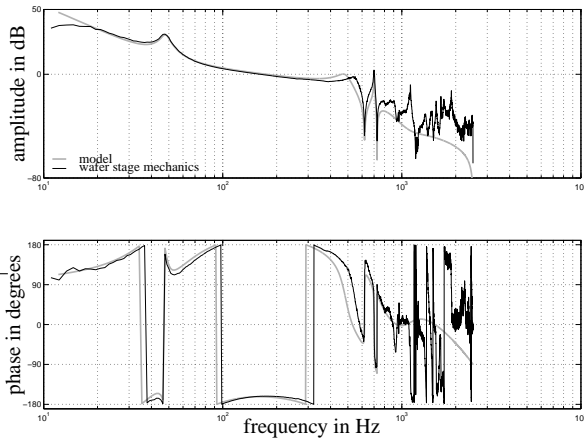


Figure 5. Bode diagram of the measured open-loop dynamics in z -direction along with the characteristics of a model.

$\mathcal{O}_L = \mathcal{C}_{fb}\mathcal{P}$ via the characteristics reconstructed from closed-loop measurement (black) along with the characteristics of a model (grey). Robust stability is sufficiently guaranteed with a controller bandwidth of \approx

160 Hz along with a phase margin of 20 degrees and a gain margin of -4.5 dB near 300 Hz.

Given the linear control design, closed-loop performance is assessed at five distinct positions on the wafer: at four wafer corner points and at the wafer center point. At each position an identical scan in terms of its acceleration x - and y -set-points is performed, the result of which is shown in Figure 6. In the error response,

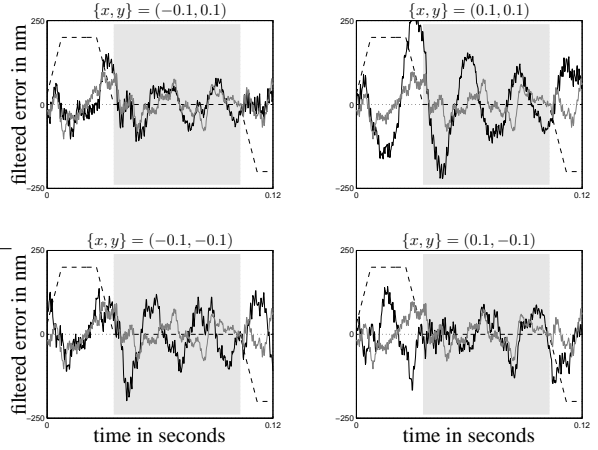


Figure 6. Time-series of the filtered error signal in z -direction under equal scans at five different $\{x, y\}$ -locations on the wafer; four corner locations (black) and a center location (grey).

large deviations can be observed at the considered positions on the wafer. Especially within the indicated interval of constant velocity. This is the interval where performance should be achieved. The differences in error response are emphasized by applying the weighting filter operation \mathcal{F}_1 , see (1), with $\beta_z = 1$, $\beta_p = 0.02$, and $\omega_z = \omega_p = 75\pi \text{ rad s}^{-1}$. It is clear that the controlled wafer stage shows position-dependent behavior, the error responses significantly differ over the wafer. Hence the kind of behavior particularly suited for the application of the hybrid control strategy.

The ability of the hybrid controller to achieve improved performance is shown in Figure 7. Still under linear closed-loop conditions (the extra nonlinear controller in Figure 2 is not yet activated) and at two scan positions: $\{x, y\} = (0.1, 0.1)$ and $\{x, y\} = (0, 0)$, the upper part of the figure shows the monitor function of the filter operation \mathcal{F}_1 applied to the error signal e along with a scaled representation of the y -acceleration set-point. The user-defined value of the deadzone length $\delta = 40 \text{ nm}$ is indicated by means of the dotted lines. At $\{x, y\} = (0, 0)$ the resulting signal almost entirely falls within the indicated bounds, whereas at $\{x, y\} = (0.1, 0.1)$ it significantly exceeds these bounds. The effect of selection through the nonlinear filter operation $\phi(\cdot)$, see (2), is shown in the middle part of the figure. For $\{x, y\} = (0.1, 0.1)$, it can be seen that the sinusoidal-based behavior largely remains unaffected whereas for $\{x, y\} = (0, 0)$ almost

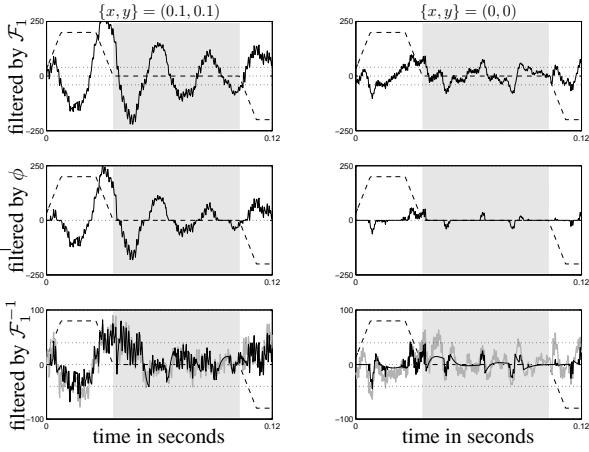


Figure 7. Time-series measurement of the closed-loop and nonlinear filtered error signals at two location on the wafer: $\{x, y\} = (0.1, 0.1)$ and $\{x, y\} = (0, 0)$ with $\delta = 40$ nm.

all (random-based) oscillations are removed from the error response. Combined with the loop-shaping function of filter \mathcal{F}_2 , see (3), the overall nonlinear filter operation gives a strong reduction of the original error signal e (black versus grey) at $\{x, y\} = (0, 0)$ whereas it roughly shows the same signal at $\{x, y\} = (0.1, 0.1)$. At $\{x, y\} = (0.1, 0.1)$, this provides the means to obtain improved disturbance suppression under high-gain feedback while at the same time it keeps the amplification of noise at $\{x, y\} = (0, 0)$ small.

4 Performance Assessment on a Wafer Stage

At a wafer stage of an industrial wafer scanner, closed-loop performance is assessed by time-series measurement and cumulative power spectral density analysis. Prior to this assessment, however, two performance measures from the wafer scanner industry are briefly discussed: overlay and fading.

Overlay is a measure for position accuracy, hence the ability to perform a new scan at a previous scan location. In terms of servo control measures, overlay is (partly) assessed by the moving average filter operation. For a time-sampled error signal $e\{i\}$ with $i \in \mathbb{Z}$, the moving average filter operation is defined as

$$\mathcal{M}_a(i) = \frac{1}{n} \sum_{j=i-n/2}^{i+n/2-1} e(j), \quad \forall i \in \mathbb{Z}, \quad (11)$$

where $n \in \mathbb{N}^+$ represents a specific time frame. Basically, (11) represents a low-pass filter operation on e .

Fading relates to image quality, hence the ability to focus light in the path from lens to wafer. Here a moving

standard deviation filter operation is used, or

$$\mathcal{M}_{sd}(i) = \sqrt{\frac{1}{n} \sum_{j=i-n/2}^{i+n/2-1} (e(j) - \mathcal{M}_a(i))^2}, \quad \forall i \in \mathbb{Z}, \quad (12)$$

that is, a rms-based high-pass filter operation.

For the previously considered wafer positions $\{x, y\} = (0.1, 0.1)$ and $\{x, y\} = (0, 0)$, improved performance with the hybrid control design is shown in Figure 8. Additionally the results are shown for the lin-

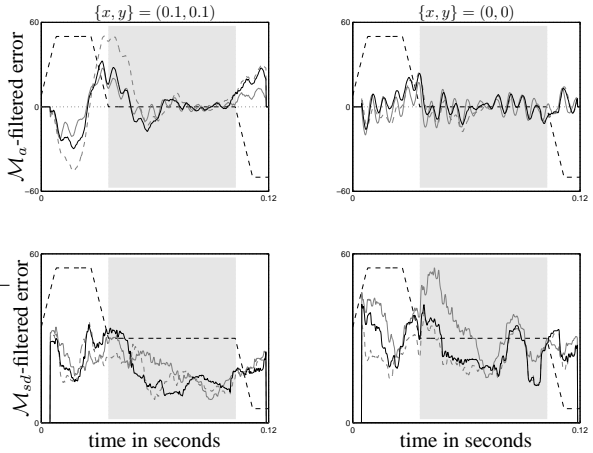


Figure 8. Time-series measurement of the \mathcal{M}_a - and \mathcal{M}_{sd} -filtered error signals at two positions $\{x, y\} = (0.1, 0.1)$ and $\{x, y\} = (0, 0)$ on the wafer.

ear design limits: the low-gain design with $\phi(\cdot) = 0$ (grey-dashed) and the high-gain design with $\phi(\cdot) = 1$ (grey-solid). In the indicated scanning interval, it can be seen in the upper-left part at $\{x, y\} = (0.1, 0.1)$ that both the hybrid design and the high-gain linear design perform equally good in terms of keeping the peak values of the moving averaged filtered error small. This shows improved low-frequent disturbance rejection in comparison with the low-gain linear design. In the lower-right part, however, at $\{x, y\} = (0, 0)$, it can be seen that both the hybrid design and the low-gain linear design perform equally good. In fact much better than the high-gain linear design. Hence an improved high-frequent noise response is obtained in comparison with the high-gain linear design.

In terms of cumulative power spectral density analysis, Figure 9 shows the results for the five considered wafer positions. A distinction is made between linear low-gain (grey-dashed), linear high-gain (grey-solid), and nonlinear gain (black-solid). It can be seen that the hybrid control design at each considered position tends to the smallest rms-value of the error signal. Note that at some positions the smallest rms-value of the error signal is determined by the linear low-gain design

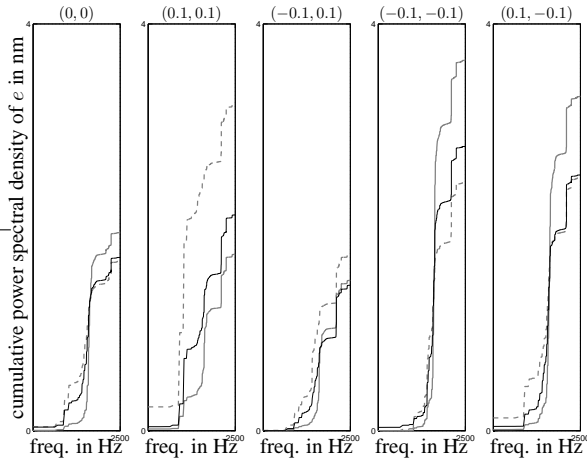


Figure 9. Cumulative power spectral density analysis of the measured servo error in z -direction at five different positions (each being the average of four realizations) on the wafer.

whereas at other positions it is determined by the linear high-gain design. The smallest versus the largest rms-values over the five wafer locations are shown in Table 2. Here it can be seen that the hybrid design

	low-gain limit	nonlinear	high-gain limit
minimum in nm	1.67	1.43	1.48
maximum in nm	3.23	2.79	3.65

Table 2. Root-mean-square (rms) values.

excels in performance either by obtaining the smallest overall rms-value but also by having the smallest error extremes. It is therefore concluded that the linear design limits cannot compete with the hybrid design in terms of servo performance along the wafer. Key is the ability to adapt the trade-off between disturbance rejection and measurement noise sensitivity according to the error response at hand.

5 Conclusions

For motion control systems, a hybrid control design is proposed which aims at improved disturbance rejection properties under equal noise response. Important is the distinction between stability and performance. While nonlinear closed-loop stability is guaranteed in the presence of loop-shaping filters, performance is effectively dealt with by the introduction of a stability-invariant weighting filter connection. For a wafer stage of an industrial wafer scanner, the hybrid controller improves upon performance in the presence of position-dependent behavior. Measured at distinct (and sufficiently distributed) positions along the wafer, the hybrid control design demonstrates improved low-frequency disturbance rejection without the necessary

transmission of high-frequency noise. The kind of transmission inherently present under high-gain feedback. In this sense, performance is achieved unknown to any linear feedback design and with expected potential in the broader field of motion control systems.

Acknowledgement

This work is partially supported by the EU Network of Excellence HYCON.

References

- Aangent WHTM, Molengraft van de MJG, and Steinbuch M. (2005) Nonlinear control of a linear motion system. In Proceedings of the 16th IFAC World Congress, Prague, Czech Republic:CD-ROM.
- Armstrong BSR, Gutierrez JA, Wade BA, and Joseph R. (2006) Stability of phase-based gain modulation with designer-chosen switch functions. *International Journal of Robotics Research*, 25:781-796.
- Baek J-S, Chung CC, and Tomizuka M. (2006) Anti-shock controller design for optical disk drive systems with a nonlinear controller. In Proceedings of the American Control Conference, Minneapolis, Minnesota:1982-1989.
- Freudenberg JS, Hollot CV, Middleton RH, and Toochinda V. (2003) Fundamental design limitations of the general control configuration. *IEEE Transactions on Automatic Control*, 48(8): 1355-1370.
- Heertjes MF, Cremers FLM, Rieck M, and Steinbuch M. (2005) Nonlinear control of optical storage drives with improved shock performance. *Control Engineering Practice*, 13:1295-1305.
- Heertjes MF, and Van de Wouw N. (2006) Variable Control Design and its Application, In Proceedings of the Conference on Decision and Control, San Diego, California, USA, pp. 3724-3729, 2006.
- Heertjes MF, and Tso T. (2007) Nonlinear Iterative Learning Control with Applications to Lithographic Machinery, *Control Engineering Practice*, doi:10.1016/j.conengprac.2007.03.005
- Mishra S, Coaplen J, and Tomizuka M. (2007) Segmented iterative learning control for nonrepetitive disturbances. *IEEE Control Systems Magazine*, August, pp. 20-25.
- Schafer RW, Oppenheim AV, Stockham TG. (1968) Nonlinear filtering of multiplied and convolved signals. In Proceedings of the IEEE, 56(8):1264-1291.
- Wal van de M, Baars van G, Sperling F, and Bosgra O. (2002) Multivariable \mathcal{H}_∞/μ feedback control design for high-precision wafer stage motion. *Control Engineering Practice*, 10:739-755.
- Yakubovich VA, Leonov GA, and Gelig AKh. (2004) Stability of stationary sets in control systems with discontinuous nonlinearities. World Scientific, Singapore.